Effect of Iron Additives on the Microstructure of Hydroxyapatite

G. A. Gamal
College of Engineering, Alqassim, Saudi Arabia
profdrgamal@qec.edu.sa

F. A. Al-Mufadi
College of Engineering, Alqassim, Saudi Arabia
almufadi@qec.edu.sa

A. H. Said
Department of Physics, South Valley University, Qena, Egypt
alaahassan2010@yahoo.com

Abstract— In this article, some Fe (III) doped hydroxyapatite samples (FeHAp) were prepared using the wet chemical method. The prepared samples were characterized via the use of X-ray diffraction (XRD) and scanning electron microscopy (SEM). Detailed structural analysis were done by Scherrer and Williamson–Hall plot methods to detect the effect of iron on the structure of hydroxyapatite (HAp). XRD patterns showed that all samples were single phased HAp. Relations between the Fe content and the deformation of the lattice parameters, dislocation density, grain size, microstrain, crystallinity were investigated. The presence of iron in the HAp lattice is found to decrease both the crystal size and the dislocation density. Further results are presented and discussed.

Keywords- Hydroxyapatite; Lattice parameters; Dislocation density; Crystallite size; Microstrain

I. INTRODUCTION

Calcium hydroxyapatite (HAp) appears now of high interest in the field of material science, since it represents the compatible inorganic component of natural bones and it can directly bond to bone in vivo. HAp is usually used as bone substitution or bone filling material, but by introducing new ions into HAp structure, new applications could be implemented. One of them is to use it as drug delivery material due to its biocompatibility, degradation, dissolution and non-toxic properties [1]. In recent years HAp was also investigated as a magnetic material for cancer treatment. It is known that heating cells up to 42 to 45 ^{o}C results in the death of cancer cells. This is usually done by delivering magnetic nanoparticles to the tumor and irradiating the particles with an AC magnetic field. Generally, HAp has many applications in both medical and engineering sciences, but further modification is needed in order to satisfy the requirements of recent applications [2].

Among the advantages of HAp is that its crystal structure is flexible due to the substituting ions. The general chemical formula of the apatites is $M_5 (YO_4)_3X$, where: M is monovalent cations (such as Na+, K+), or divalent cations (such as Ca^{2+}, Sr^{2+}, Ba^{2+}, Mg^{2+}, Cd^{2+}, Pb^{2+}, etc.), or trivalent cations (such as Na^{+}, K^{+}, Al^{3+}, Fe^{3+}, Fe^{2+}, La^{3+}, etc.) , X=univalent anion (such as OH^{-}, F^{-}, Cl^{-}, Br^{-}, or $CO3^{2-}$) and $YO_4 = (PO_4^{3-}, VO_4^{3-}, AsO_4^{3-}, SiO_4^{4-}, CO_3^{2-})$ [3].

It is an established fact that substitution of iron ions in the crystal structure of hydroxyapatite affects its physical and biological properties. Morrissey et al [4] studied the influence of Fe (II) ions on the structural properties of HAp prepared by the wet chemical reaction with diammonium hydrogen phosphate, calcium nitrate and ferrous nitrate solution. Filho et al [5] studied the effect of iron oxide concentration and the influence of heat treatment on the microhardness of hydroxyapatite. Kuda et al [6] found that the addition of iron or magnetite to biogenic hydroxyapatite makes it possible to produce magnetic biocomposites. The magnetic properties of such materials depend on the type and amount of additives. Yan Li et al [7] reported that Fe3+ doped HAp showed paramagnetic properties and the magnetic susceptibility increased with the increase of Fe3+ content. Recently Mirestean et al [8] prepared hydroxyapatite doped with different iron concentrations by the sol–gel method and stated that it can be used for hyperthermia treatment of bone tumors. Nakahira et al [1] synthesized hydroxyapatite doped with iron for drug delivery system (DDS). Various papers have been recently published on the continuous improvement of HAp, focusing on the limitations to low load bearing applications or on physical properties. This is evident from the work of Li et al [9] for synthesis and cytocompatbility of manganese (II) and iron (III) substituted HAp nanoparticles, Kai et al [10] who studied the synthesis and magnetic property of iron ions–doped HAp and the investigation of synthesis and HA nanoparticles with tailorable morphologies and carbonate substitutions using a wet precipitation method done by Fei et al [11].

The present work aims to investigate the effect of iron additives on the structural properties of hydroxyapatite.

II. EXPERIMENTAL PROCEDURE

A. Synthesis of Pure Hydroxyapatite and Fe3+ doped Hydroxyapatite

Five samples of hydroxyapatite were synthesized via the wet chemical method [12, 13]. The chemical reagent and starting materials concentrations for the precipitation are listed in Table I. In order to avoid tedious details about sample preparations, Figure 1 illustrates the preparation procedure.

TABLE I. CHEMICAL REAGENT OF THE PREPARED SAMPLES.

Sample	Code	$Ca(No_3)_2.4H_2O$		$(NH_4)_2HPO_4$		$Fe(No_3)_3.9H_2O$	
		gm	Mol	gm	Mol	gm	Mol
1	HAp	36.8	0.16	12.66	0.096	-----	-----
2	$FeHAp_1$	36.8	0.16	12.66	0.096	2.02	0.005
3	$FeHAp_2$	36.8	0.16	12.66	0.096	4.04	0.01
4	$FeHAp_3$	36.8	0.16	12.66	0.096	8.08	0.02
5	$FeHAp_4$	36.8	0.16	12.66	0.096	12.12	0.03

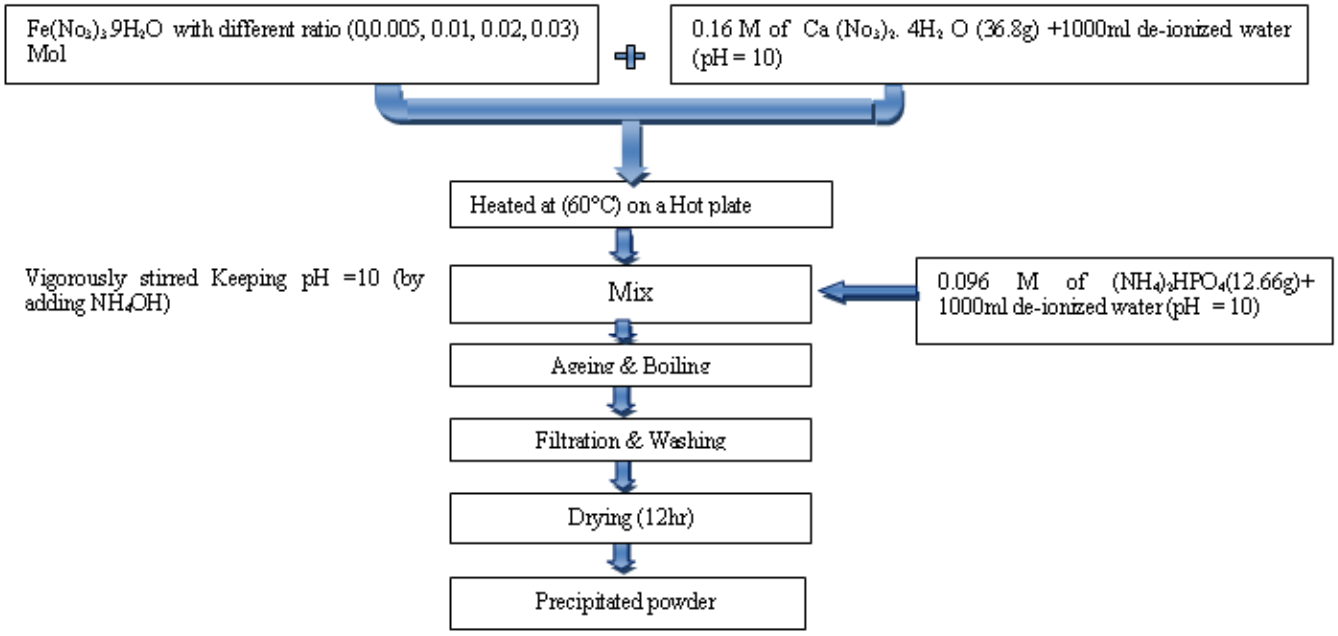

Fig. 1. Flow chart of the preparation technique

B. Scanning electron microscope (SEM)

The morphology of the prepared samples was examined using a JEOL SEM model JSM-5500-Japan, with 10 kV accelerating voltage.

C. X-ray diffraction

X-ray diffraction (XRD) pattern data were obtained at room temperature for the prepared samples using the powder technique in an X'Pert PRO-PAN analytical diffractometer (with Cu-Kα radiation, λ= 1.54056A˚) at 40 kV and 30 mA. Intensity data were collected by the step-counting method (step 0.020 and a time per step of 0.4 s) between 10˚ and 80˚ for (2θ) as illustrated in Figure 2 where θ is the angle between the incident ray and the scattering planes.

The lattice parameters were calculated by the following formula [14].

$$\frac{1}{d^2} = \frac{4}{3}\left[\frac{h^2 + hk + k^2}{a^2}\right] + \frac{l^2}{c^2} \qquad (1)$$

Where *d* is the interplanar spacing, *hkl* are miller's indices and *a* and *c* are lattice parameters. For determination of the unit cell volume, the following formula is used [14]:

$$V = \frac{\sqrt{3}}{2} a^2 \cdot c \quad (2)$$

Also the crystallinity of the studied samples is calculated with the aid of the following equation [15]:

$$X_c = 1 - \frac{V_{112/300}}{I_{300}} \quad (3)$$

Where X_c is the percentage of crystallinity degree, $V_{112/300}$ is the intensity of the hollow between (112) and (300) diffraction peaks, I_{300} is the intensity of (300) diffraction peak. The size of the crystallites responsible for the Bragg reflection of the (002), (112), (211) and (300) planes were determined using the well-known Scherrer relationship [16]:

$$\Gamma = \frac{0.94\,\lambda}{D\cos\theta} \quad (4)$$

Where Γ is the full width at half-maximum (FWHM) and D is the crystal size.

Williamson Hall technique takes into account both size and strain effects. This method provides estimation for the crystal size D as well as for the micro-strain ε as follows [17]:

$$\Gamma\cos\theta = \frac{0.9\lambda}{D} + 4\varepsilon\sin\theta \quad (5)$$

The above formula between $\Gamma\cos\underline{\theta}$ and $\sin\theta$ is a linear relationship as predicted. From the intercept of the line we can have the crystal size. The slope of the fitted line provides the micro-strain.

The average dislocation density ρ can be determined from the following equation [18]:

$$\varepsilon^2 = (\pi A b^2/2)\, R_e C \quad (6)$$

Where $(b^2/2)$ is the Burgers vector, A is a constant defined by the effective outer cut-off radius of dislocations (Re) and C is the contrast factor.

III. RESULTS AND DISCUSSIONS

A. Scanning electron microscopy

SEM is used to examine the morphology of the studied samples and to show the effect of the substitution process on the structure of HAp. Two magnifications were used for all samples X 50 with magnification bar 500 µm and X 1000 with magnification bar 10 µm. Red circles illustrate the HAp particle agglomeration at different Fe concentrations.

The effect of substitutions on the structure of HAp leads to a decrease in the grain size as the concentration of iron increase. This is attributed to the smaller ionic radius of iron compared with that of calcium as seen in Figures [2(a), 3 (a), 4 (a), 5 (a), 6 (a)]. This is in complete agreement with the results obtained from XRD.

The formation mode of HAp particles appears as spherical particles agglomerated together as indicated in Figures [2 (b), 3 (b), 4 (b), 5 (b), 6 (b)].

B. XRD

Phase identification was done via the XRD method. Figure 7 shows the XRD patterns of all prepared samples. Present peaks agree with ICSD (Inorganic Crystal Structure Database) card no.76-694 [19] and none of the patterns displayed extra peaks indicating that all samples are single phased HAp. Also it is concluded that the grown phase is a hexagonal system with a space group P6/3m.

The effect of substitutions in HAp structure is appeared in the XRD chart as a change in the peak position, intensity and broadening. From XRD we can observe that there is a slight shift of the peak position in all iron doped HAp samples compared with pure HAp and also that the peak intensity of all samples is smaller than of that of pureHAp. This may be attributed to the smaller particle size and greater structural strain in the metal cations doped HAp relative to pure HAp.

For more utilization of Figure 2, we shall digress with an illustration of the width of the main peak in case of five samples. So, software and computational treatments yields the obtained histogram shown in Figure 8. Except for the case of Fe^{3+} concentration of 0.3, it evident that the quantity (the full width at half maximum) rises as the Fe^{3+} increases. The significance of this observation is that substitution of Fe^{3+} causes some kind of defects in the crystal arrays i.e. with the increment of Fe^{3+} substitution the obtained crystal becomes more defective.

The obtained values of unit cell parameters (a, c) and unit cell volumes are listed in Table II.

Since the ionic radius of Fe^{3+} (0.64 A˚) is smaller than that of Ca^{2+} (0.99 A˚), therefore it is logical that the substitution of Fe for Ca causes a decrease in either or both lattice parameters. Figure 9 shows the variation of both lattice parameters (a, c) and the unit cell volume with the concentration of the substituted iron. We can see a slight decrease in both lattice parameters and unit cell volume as the concentration of Fe increases, for all iron doped HAp samples in comparison to pure HAp.

This indicates that Fe substituted for Ca caused shrinking to the HAp crystal. A similar behaviour was observed in a previous work with cations smaller than Ca such as (Mg^{2+}, Zn^{2+}, In^{3+}, Y^{3+}), while an expansion also observed with cations larger than Ca such as (Bi^{3+}, La^{3+}) [14]. In spite of the clear decrease in both lattice parameters he unit cell volume, one can't exclude the impression that there is an evident fluctuation in the recorded lattice parameter values.

The fluctuation in the lattice parameter may be attributed to:

- The substitution range of Fe3+ as the probability of substitution changed from one sample to another.
- The effect of carbonate substitution as the carbonate anion enters the HAp lattice by substituting for either hydroxyl or phosphate anions.

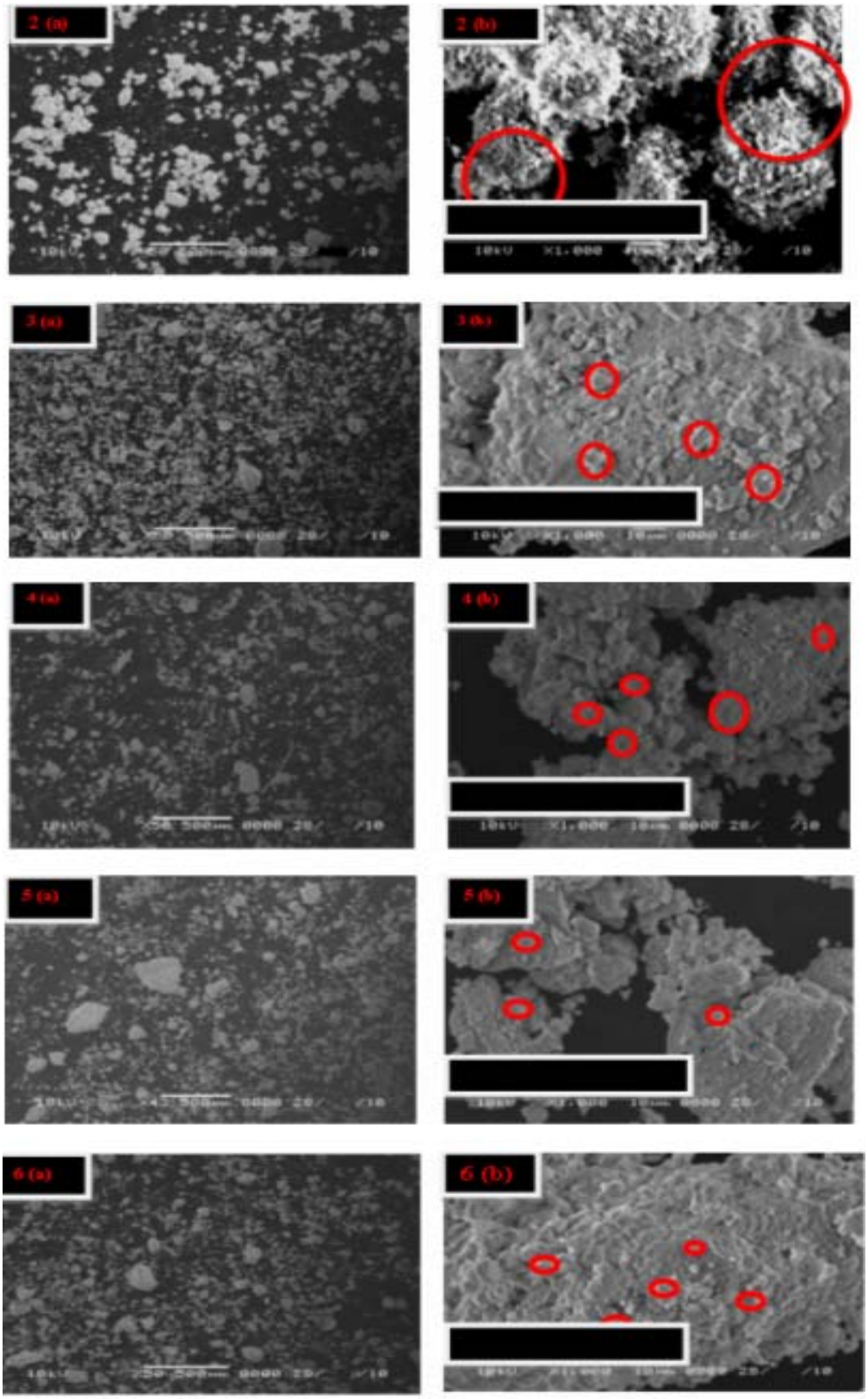

Fig. [2(a), 3(a), 4(a), 5(a), 6(a)]- SEM of HAp, $FeHAp_1$, $FeHAp_2$, $FeHAp_3$ and $FeHAp_4$ samples with magnification bar 500 µm.
Fig. [2(b), 3(b), 4(b), 5(b), 6(b)]- SEM of HAp, $FeHAp_1$, $FeHAp_2$, $FeHAp_3$ and $FeHAp_4$ samples with magnification bar 1000 µm

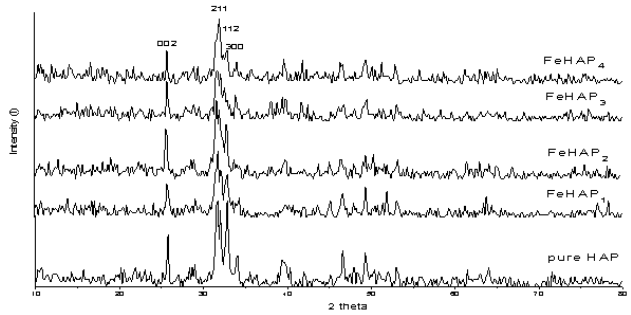

Fig. 7. XRD patterns of pure HAp and Fe substituted HAp

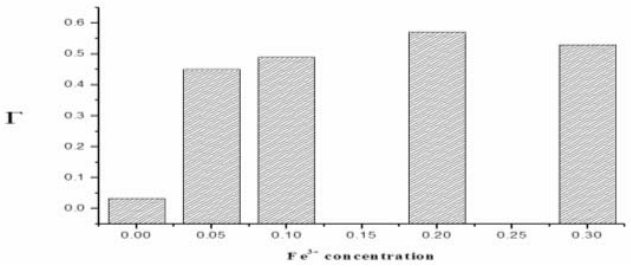

Fig. 8. The full width at half-maximum of the main peak as a function in Fe content

TABLE II. LATTICE PARAMETER AND UNIT CELL VOLUME OF THE PREPARED SAMPLES

Samples		Plane	d (Å)	Parameter (Å)	Average (Å)	Unit cell volume (Å)^3
HAp	A	300	2.718	9.416	9.410	528.190
		211	2.810	9.405		
	C	002	3.443	6.887	6.886	
		004	1.721	6.885		
FeHAp1	A	300	2.711	9.416	9.369	521.989
		211	2.794	9.345		
	C	002	3.431	6.862	6.866	
		004	1.717	6.869		
FeHAp2	a	300	2.715	9.405	9.399	526.7005
		211	2.807	9.392		
	c	002	3.445	6.890	6.883	
		004	1.719	6.877		
FeHAp3	a	300	2.706	9.376	9.380	523.411
		211	2.804	9.384		
	c	002	3.433	6.866	6.868	
		004	1.717	6.869		
FeHAp4	a	300	2.716	9.409	9.404	527.138
		211	2.808	9.400		
	c	002	3.438	6.876	6.881	
		004	1.721	6.886		

Depending on the deviations in the lattice constants, the position of the substitution can be determined. It is established that the substitution of carbonate anion for the phosphate anion, provokes an expansion in the unit cell length along the c-axis and a contraction along the a-axis. Whereas, the substitution of carbonate for the hydroxyl group is induced and causes an expansion along the a-axis and a contraction on the c-axis [20].

In the prepared samples under study both types of carbonates are expected, which means that the two possibilities are expected too.

For a detailed study about this point and in order to find out the influence of Fe^{3+} substitution on the crystal size we applied (4). Table III shows the average crystal size of all samples calculated by (4) due to the peaks from (002), (112), (211), (300) reflection planes. The values of the crystal sizes for all samples ranged from 26.8 to 18 A°. The effect of iron in the crystal size can be observed easily via the decrease of the crystal size of all iron doped samples compared to pure HAp as indicated in Table III and Figure 10. This may be attributed to the smaller ionic radius of iron that causes a shrinking to the HAp. These results confirm the reduction observed in the cell parameters and volume values as seen in Figure 9.

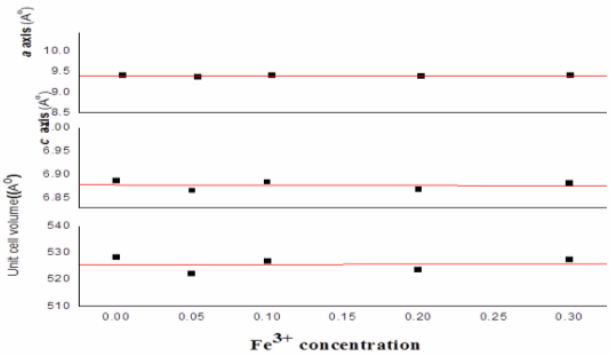

Fig. 9. Lattice parameters (a) a axis, (b) c axis and (c) unit cell volume as a function of iron concentration.

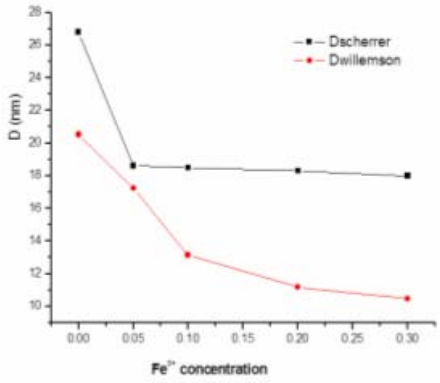

Fig. 10. The calculated crystal size *D* from Scherrer and Willimson-Hall equations as a function of Fe content.

Another method for finding D is the Williamson- Hall relation. Figure 10 also shows the corresponding estimated values of crystal size D. Regarding (5), it was utilized because it takes into account that the total width of the x-ray diffraction peak is due to both size and strain effects. For the separation, the different dependence is helpful: the size broadening is proportional to $\cos^{-1}\theta$ and the strain broadening is proportional to $\tan\theta$. Accordingly plotting the relation between $\Gamma\cos\theta$ and $\sin\theta$, we can get from the intercept the value of D and from the slope the value of ε (the micro- strain).

The crystallinity of the five samples is deduced with the aid of (3). Variation of the crystallinity against the Fe concentration is depicted in Figure 11. The general mode of variation of Fe content against the crystallinity is the decrease of the crystallinity and/or the increase in the lattice imperfections [21] as Fe content increases. The degree of crystallinity of HAp ceramics can be influenced by many factors such as preparation methods, heat treatment, crystal size and substitutions. Presently we believe that the effect of decreasing the crystal size is the factor responsible for decreasing the crystallinity of the prepared samples. This is supported with the XRD spectra where a broadening of diffraction peaks is noticeable as the Fe^{3+} increases. These results agree with the observations in [7, 22]. Also one can't exclude the role played by doping of iron ions which inhibited the c-axis growth and promoted the a-axis growth as concluded in [10].

The effect of substitutions can vary according to the amount and the type of the substituted ions. For example Mg^{+2} can cause a decrease in the crystallinity of HAp [15] while the substitutions of fluoride (F^- for OH^-) can cause an increase in the crystallinity [23]. Also the substitution of carbonate in β position reduces the stability and crystallinity of HAp, since vacancies in calcium site will be formed in order to re-equilibrate the change neutrality [24].

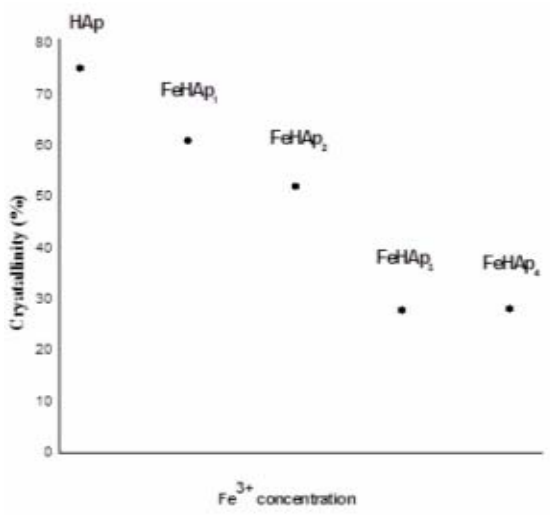

Fig. 11. Effect of iron content on the XC%in the studied samples.

TABLE III. CALCULATED CRYSTAL SIZE OF THE PREPARED SAMPLES

Sample	D (nm) Scherrer	D (nm) Williamson-Hall	ε
HAp	26.8	20.5	9.75 E-4
FeHAp1	18.6	17.2	19.9 E-4
FeHAp2	18.5	13.1	12.2 E-4
FeHAp3	18.3	11.1	5.37E-4
FeHAp4	18	10.4	9.17E-4

Now it is clear that D decreases as Fe^{3+} is increased. This is true for D estimated by Scherrer or even by Williamson-Hall relations. From the results of the crystal size and microstrain measurements of the prepared samples shown in Table III we can note that:

- The average crystal size measured by Scherrer equation is larger than that measured from Williamson- Hall plot. Thus, apparently, the Scherrer method overtimes the crystal size likely due to the fact that it does not separate broadening due to the strain in the lattice from that due to refined grain structure [25].
- There are strains and lattice distortions in our samples, which mean that our samples may have dislocations [26].

For better understanding of the nature of the relation between D and ε and Fe^{3+} concentration, Figure 13 is constructed. This was done on the basis of (5). A set of straight lines (as expected) were obtained as illustrated in Figure 12.

From the intercepts we computed values of ε as listed in Table III. So, Figure 13 depicts the relation between ε and Fe^{3+} concentration. From Figure 13 it is seen that the relation between ε and Fe^{3+} concentration is decreasing linearly. This reflects the fact that as the amount of Fe substitution increases, the HAp sample tends to be more mechanically stable. Because of the availability of ε values at different Fe^{3+} concentrations and by using (6), dislocation densities can be obtained at that condition. Accordingly, Figure 14 is drawn.

One sees the trend line for the dislocation density decreasing gradually as a function of Fe^{3+} concentration. This conclusion is rather surprising since we concluded from Figure 8 that the width of the x-ray main peak increases (indicating that more Fe^{3+} yields more defects). Also the crystallinity was decreased as Fe^{3+} increased. Here dislocations are decreasing as Fe^{3+} concentration increases. In the mean time, it seems that the generation of another type of defects (point or line defects) as a result of Fe^{3+} concentration increases.

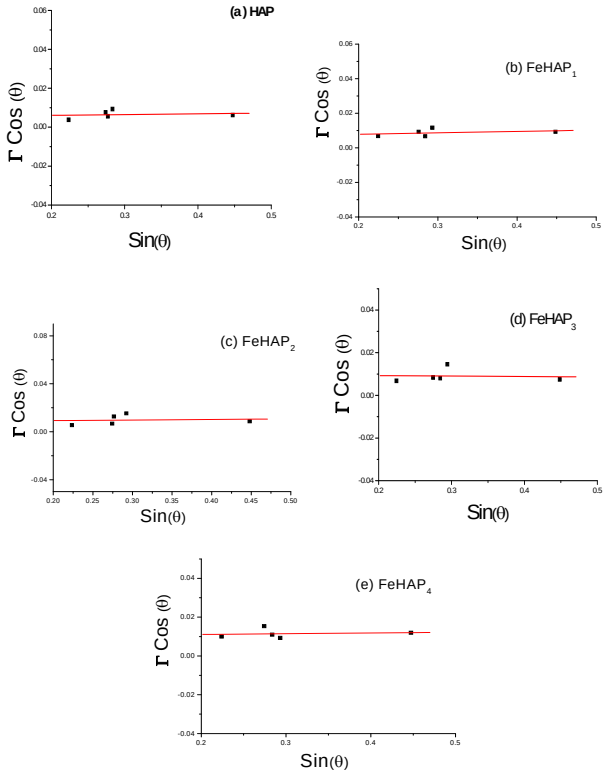

Fig. 12. The Williamson Hall plot of the prepared samples (a) HAp, (b) FeHAp1, (c) FeHAp2, (d) FeHAp3 and (e) FeHAp4 respectively

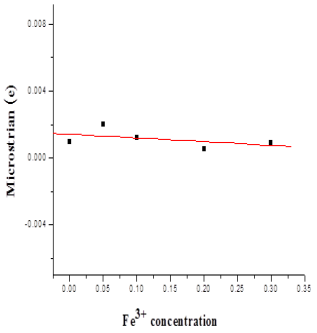

Fig. 13. The calculated microstrian of the prepared samples as a function in Fe content.

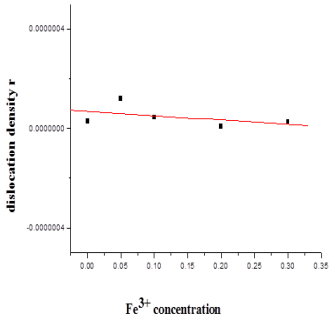

Fig. 14. The calculated dislocation density of the prepared samples as function in Fe content.

IV. CONCLUSION

Some Fe^{3+} doped HAp samples were prepared by the wet chemical method. The influence of iron additives on the microstructure of the prepared samples was studied. Detailed study was done using the X-ray and SEM methods. Scherrer and Williamson–Hall relations were employed to detect the effect of Fe^{3+} introduction in Hap structure. Definite results were obtained as Fe^{3+} concentration increase:

1. The width of the main x-ray peak was broadening indicating a generation of new defects inside the samples.
2. The crystallinity decreases as a result of doping of iron ions.
3. From Scherrer and Williamson–Hall data it was found that crystal size *D* decreased. This was attributed to the smaller ionic radius of iron that causes shrinking of the unit cell volume.
4. The dislocation densities were decreased.
5. Combining point 4 with the x- ray peaks broadening and the crystallinity decrease, we concluded a generation of other defects (point or line) as Fe^{3+} is substituted in HAp.

Appearance of the point defects instead of the dislocations opens up new possibilities for modern use of the iron substituted HA as a hard, strong and durable material.

REFERENCES

[1] A Nakahira, S Nakamura, M. Horimoto, "Synthesis of modified hydroxyapatite (HAP) substituted with fe ion for DDS application", IEEE Transactions on Magnetics, Vol. 43, No. 6, pp. 2465-2467, 2007

[2] C. Hou, S. Hou, Y. Hsueh, J. Lin, H. Wu, F. Lin, "The in vivo performance of biomagnetic hydroxyapatite nanoparticles in cancer hyperthermia therapy", Biomaterials, Vol. 30, No. 23-24, pp. 3956-3960, 2009

[3] W. Pon-On, S. Meejoo, I. Tang, "Incorporation of iron into nano hydroxyapatite particles synthesized by the microwave process", International Journal of Nanoscience, Vol. 6, No. 1, pp. 9-16, 2007

[4] R, Morrissey, L. M. Rodriguez-Lorenzo, K. A. Gross, "Influence of ferrous iron incorporation on the structure of hydroxyapatite", Journal of Materials Science: Materials in Medicine, Vol. 16, No. 5, pp. 387-392, 2005

[5] F. P. Filho, R. E. F. Q. Nogueira, M. P. F. Graca, M. A. Valente, A. S. B. Sombra, C. C. Silva, "Structural and mechanical study of the sintering effect in hydroxyapatite doped with iron oxide", Physica B: Condensed Matter, Vol. 403, No. 19-20, pp. 3826-3829, 2008

[6] O. Kuda, N. Pinchuk, L. Ivanchenko, O. Parkhomey, O. Sych, M. Leonowicz, R. Wroblewski, E. Sowka, "Effect of Fe_3O_4, Fe and Cu doping on magnetic properties and behaviour in physiological solution of biological hydroxyapatite/glass composites", Journal of Materials Processing Technology, Vol. 209, No. 4, pp. 1960-1964, 2009

[7] Y. Li, C. T. Nam, C. P. Ooi, "Iron (III) and manganese (II) substituted hydroxyapatite nanoparticles: characterization and cytotoxicity analysis", Journal of Physics: Conference Series, Vol. 187, No. 012024, pp. 1-8, 2009

[8] C. Mirestean, H. Mocuta, R. V. F. Turcu, G. Borodi, S. Simon, "Nanostructurated materials for hyperthermia treatment of bone tumors", Journal of Optoelectronics and Advanced Materials, Vol. 9, No. 3, pp. 764-767, 2007

[9] Y. Li, J. Widodo, S. Lim, C. P. Ooi, "Synthesis and cytocompatibility of manganese (II) and iron (III) substituted hydroxyapatite nanoparticles", Journal of Materials Science, Vol. 47, No. 2, pp. 754-763, 2012

[10] K. Zuo, Y. Zeng, D. Jiang, "Synthesis and magnetic property of iron ions-doped hydroxyapatite", Journal of Nanoscience and Nanotechnology, Vol. 12, No. 9, pp. 7096-7100, 2012

[11] F. Peng, E. Veilleux, M. Schmidt, M. Wei, "Synthesis of hydroxyapatite nanoparticles with tailorable morphologies and carbonate substitutions using a wet precipitation method", Journal of Nanoscience and Nanotechnology, Vol. 12, No. 3, pp. 2774-2778, 2012

[12] I. Mayer, O. Jacobsohn, T. Niazov, J. Werckmann, M. Iliescu, M. Richard-Plouet, O. Burghaus, D. Reinnen, "Manganese in Precipitated Hydroxyapatites", European Journal of Inorganic Chemistry, Vol. 2003, No. 7, pp. 1445-1451, 2003

[13] E Gyorgy, P. Toricelli, G. Socol, M Iliescu, I Mayer, I. N. Mihailescu, A. Bigi, J. Werckmann, "Biocompatible Mn^{2+}-doped carbonated hydroxyapatite thin films grown by pulsed laser deposition", Journal of Biomedical Matterials Research, Vol. 71A, No. 2, pp. 353-358, 2004

[14] T. J. Webster, E. A. Massa-Schlueter, J. L. Smith, E. B. Slamovich, "Osteoblast response to hydroxyapatite doped with divalent and trivalent cations", Biomaterials, Vol. 25, No. 11, pp. 2111-2121, 2004

[15] I. Cacciotti, A. Bianco, M. Lombardi, L. Montanaro, "Mg-substituted hydroxyapatite nanopowders: Synthesis, thermal stability and sintering behaviour", Journal of the European Ceramic Society, Vol. 29, No. 14, pp. 2969-2978, 2009

[16] C. Suryanarayana, M. Grant Norton, X-Ray Diffraction: A Practical Approach, Springer, 1998.

[17] A. A. Ebnalwaled, M. Abou Zied, "Microstructure and mechanical properties of Nano-crystalline Al-Mg-Mn system", Journal of Nano Research, Vol. 9, pp. 61-68, 2010

[18] M. Wilkens, "The determination of density and distribution of dislocations in deformed single crystals from broadened X-ray diffraction profiles", Physica Status Solidi A, Vol. 2, No. 2, pp. 359-370, 1970

[19] T. Leventouri, C. E. Bunaciu, V. Perdikatsis, "Neutron powder diffraction studies of silicon-substituted hydroxyapatite", Biomaterials, Vol. 24, No. 23, pp. 4205-4211, 2003

[20] L. Borum-Nicholas, O. C. Wilson Jr, "Surface modification of hydroxyapatite. Part I. Dodecyl alcohol", Biomaterials, Vol. 24, No. 21, pp. 3671-3679, 2003

[21] C. C. Ribeiro, I. Gibson, M. A. Barbosa, "The uptake of titanium ions by hydroxyapatite particles-structural changes and possible mechanisms", Biomaterials, Vol. 27, No. 9, pp. 1749-1761, 2006

[22] J. Wang, T. Nonami, K. Yubata, "Syntheses, structures and photophysical properties of iron containing hydroxyapatite prepared by a modified pseudo-body solution", Journal of Materials Science: Materials in Medicine, Vol. 19, No. 7, pp. 2663-2667, 2008

[23] P. Guggenbuhl, R. Filmon, G. Mabilleau, M. F. Basle, D. Chappard, "Iron inhibits hydroxyapatite crystal growth in vitro", Metabolism, Vol. 57, No. 7, pp. 903-910, 2008

[24] E. Landi, G. Celotti, G. Logroscino, A. Tampieri, "Carbonated hydroxyapatite as bone substitute, Journal of the European Ceramic Society, Vol. 23, No. 15, pp. 2931-2937, 2003

[25] M. S. Choudry, M. Dollar, J. A. Eastman, "Nanocrystalline NiAl-processing, characterization and mechanical properties", Materias Science and Enginerring A, Vol. 256, No. 1-2, pp. 25-33, 1998

[26] W. A. Jesser, D. Kuhlmann-Wilsdorf, "On the theory of interfacial energy and elastic strain of epitaxial overgrowths in parallel alignment on single crystal substrates", Physica Status Solidi B, Vol. 19, No. 1, pp. 95–105, 1967